ISSN 0208-7774 TRIBOLOGIA 3/2019 p. 51–59
DOI: 10.5604/01.3001.0013.5434

Waldemar KARASZEWSKI*

ANALYSIS OF RING CRACKS IN CERAMIC ROLLING ELEMENTS USING THE BOUNDARY ELEMENT METHOD

ANALIZA PĘKNIĘĆ KOLISTYCH W CERAMICZNYCH ELEMENTACH TOCZNYCH METODĄ ELEMENTÓW BRZEGOWYCH

Key words: crack propagation, ceramic materials, ball bearings, numerical analysis.

Abstract

Ceramic materials have been increasingly used in bearing systems for over a dozen years. This is due to the specific properties of ceramic materials, such as high hardness, corrosion resistance, the possibility of use in aggressive chemical environments, as well as due to the lower specific weight as compared to steel materials. However, the use of ceramic materials imposes many limitations. The main disadvantages include surface cracks and a low fracture toughness value.

The paper presents a numerical analysis of crack propagation in silicon nitride balls. The directions of propagation were analysed for the cracks that are most commonly found on the surface of the commercially available ceramic balls. The directions were analysed along the crack front and considering the location of the crack in relation to the contact point of the balls in the rolling contact. The numerical calculations are based on a three-dimensional model of the ring crack. Numerical calculations were carried out using the boundary element method. Numerical solutions were compared with the results of experimental research.

Słowa kluczowe: propagacja pęknięć, materiały ceramiczne, łożyska toczne, analiza numeryczna.

Streszczenie

Materiały ceramiczne od kilkunastu lat znajdują coraz większe zastosowanie w układach łożyskowych. Wynika to z charakterystycznych właściwości materiałów ceramicznych takich jak: duża twardość, odporność na korozję, możliwość stosowania w środowiskach agresywnie chemicznych, a także z uwagi na mniejszy ciężar właściwy w porównaniu z materiałami stalowymi. Stosowanie materiałów ceramicznych wiąże się jednak z wieloma ograniczeniami. Głównymi ich wadami są pęknięcia powierzchniowe oraz niska odporność na kruche pękanie.

W pracy przedstawiono analizę numeryczną propagacji pęknięć w kulkach ceramicznych wykonanych z azotku krzemu. Analizowano kierunki propagacji dla pęknięć kolistych, które najczęściej spotykane są na powierzchni handlowych kulek ceramicznych. Kierunki pęknięć analizowano wzdłuż czoła pęknięcia oraz względem położenia pęknięcia w stosunku do punktu styku współpracujących kulek w styku tocznym. Obliczenia numeryczne oparte zostały na trójwymiarowym modelu pęknięcia kolistego. Obliczenia numeryczne analizowano metodą elementów brzegowych. Rozwiązania numeryczne porównano z wynikami badań eksperymentalnych.

INTRODUCTION

The technological development and efforts to extend the operating life and the reliability of machinery and equipment, in many cases, make it more difficult for the conventional ball bearings to meet specific requirements. By using literature and author's own observations, it is possible to define the directions in ball bearing development, leading to the following:

- Reducing friction,
- Providing a specified long service life (increase in the number of available operating hours),
- Increasing load-bearing capacity,

* ORCID: 0000-0003-3085-9468. Gdańsk University of Technology, Faculty of Mechanical Engineering, Narutowicza 11/12 Street, 80-233 Gdańsk, Poland, e-mail: walkaras@pg.edu.pl.

- Reducing centrifugal forces in high RPM applications,
- Protecting the environment, and
- Increasing corrosion resistance during operation in aggressive environments.

However, the most promising opportunities are provided by using high-tech ceramic materials. Currently, both full ceramic and hybrid bearings are manufactured. Especially the latter ones whose steel races cooperate with ceramic rolling elements are more and more commonly used in various industry sectors. The high interest in rolling bearings made of ceramic materials results from the advantageous properties of this material group. Currently manufactured hybrid rolling bearings contain rolling elements made of silicon nitride, while full ceramic rolling bearings are most frequently made of aluminium oxide or zirconium dioxide.

Particularly high hopes are held for using ceramic materials in rolling contacts exposed to high loads, including rolling bearing elements. The service life of currently used ceramic bearings is about five times higher than in the case of comparable metal rolling bearings. Nevertheless, when selecting ceramic rolling bearings, special attention should be paid to their advantageous properties and primarily to any occurrence of surface damage. The damage can result from ceramic structure flaws that appear during the manufacturing process, but it can also occur during operation (e.g., cracks caused by shock loads). This sort of damage and its propagation resulting from fatigue loads during operation is a significant component that reduces the life of ceramic rolling elements, and therefore, also the life of whole bearings. It applies both to full ceramic and hybrid bearings **[L. 1–3]**.

NUMERICAL ANALYSIS USING THE BOUNDARY ELEMENT METHOD (BEM)

The dual boundary element method (BEM) has been used for numerical analysis in fracture mechanics for many years. This paper uses this technique to analyse cracks in ball bearings made of silicon nitride with Beasy utility program **[L. 3, 4]**. The method allows one to do the following:

- Calculate the values of stress intensity factor,
- Determine the direction of ring cracks, and
- Determine the shape of propagating gap.

This paper presents a numerical analysis of crack propagation direction in spherical ceramic balls made of silicon nitride. The experimental studies of ceramic balls in rolling contact **[L. 6, 7]** reveal that the direction of crack propagation significantly affects the service life of this combination. The most dangerous situation is when the initial crack propagates towards the ceramic ball surface. The propagating crack, the "secondary crack," after reaching the surface, causes its sudden damage by "chipping away" large material "pieces" from the area between primary and secondary crack. Therefore, the knowledge of crack propagation direction is important, since it affects the life of ceramic material combinations in a rolling contact.

The advantage of the dual boundary element method (BEM) is the fact that it eliminates the need for redividing material into boundary elements while analysing subsequent crack increments. The analysis includes only the new elements that model the propagating crack.

Figure 1 presents a BEM model of two contacting balls, 12.7 mm in diameter, that simulates a contact

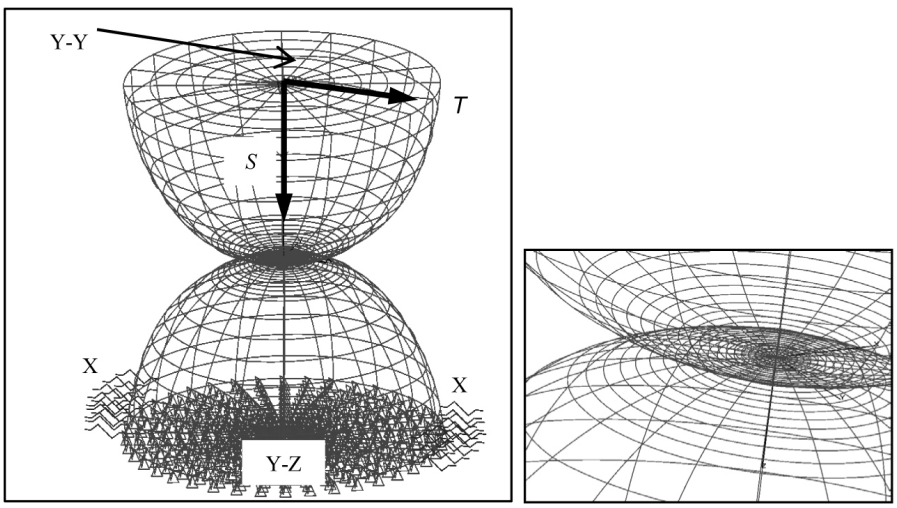

Fig. 1. The boundary conditions for the contact of two balls – BEM model (*S* – vertical force at the interface between two balls, *T* – traction force, Y-Z – surface, where displacement in y-z plane was detected, X – elastic elements acting along the x axis, Y-Y – plane, where displacement in direction y was detected

Rys. 1. Warunki brzegowe dla kontaktu dwóch kulek – model MEB (*S* – siła pionowa w styku dwóch kulek, *T* – siła trakcyjna, Y-Z – powierzchnia, na której odebrane zostało przemieszczenie w płaszczyźnie y-z, X – elementy sprężyste działające wzdłuż osi x, Y-Y – płaszczyzna, w której odebrano przemieszczenie w kierunku y

interface in the experimental studies performed **[L. 6, 8]**. Before the BEM analysis with introduced cracks, a contact simulation for various BEM grid densities was performed to find if the numerical solution was consistent **[L. 6]**. The numerical analysis of boundary element method was performed for Si_3N_4/bearing steel combinations with the interface of combined balls subjected to a load of 306 N. The maximum contact pressure in the ball interface for the above mentioned load is 4.8 GPa. **Table 1** presents material data for silicon nitride and bearing steel as assumed in the analysis.

The shape shown in **Fig. 2** was assumed as a crack model. The shape of the crack and the division into elements was adjusted to make the numerical solution consistent **[L. 6]**. The assumed crack model is shown in **Fig. 3**, while **Fig. 4** presents the crack model grid introduced in the ceramic ball under analysis.

Table 1. Material data for silicon nitride and bearing steel and the values of loads assumed in numerical calculations
Tabela 1. Dane materiałowe azotku krzemu i stali łożyskowej oraz wartości obciążeń przyjęte w obliczeniach numerycznych

Data	Si_3N_4/steel combination
Load (vertical force at the interface of two balls) S [N]	306
Traction force T [N]	15.3
Ball radius $r_1 = r_2$ [mm]	6.35
Young's modulus E_1 [N/mm^2] (silicon nitride)	324,000
Young's modulus E_2 [N/mm^2] (bearing steel)	208,000
Count v_1 [−] (silicon nitride)	0.27
Count v_2 [−] (bearing steel)	0.30

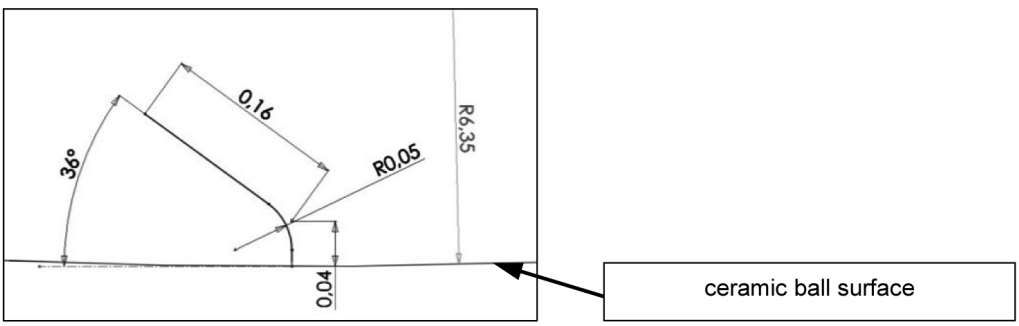

Fig. 2. Dimensions of the assumed crack model [L. 5, 7]
Rys. 2. Wymiary przyjętego modelu pęknięcia **[L. 5, 7]**

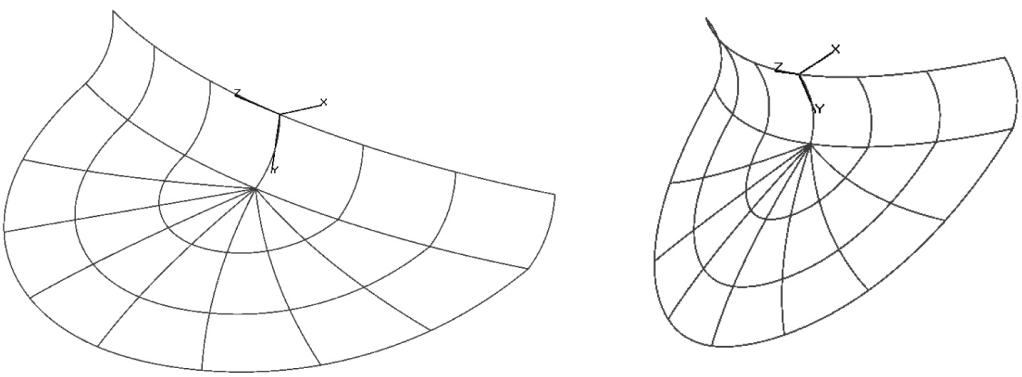

Fig. 3. Model of a ring crack (boundary element method)
Rys. 3. Model pęknięcia kolistego (metoda elementów brzegowych)

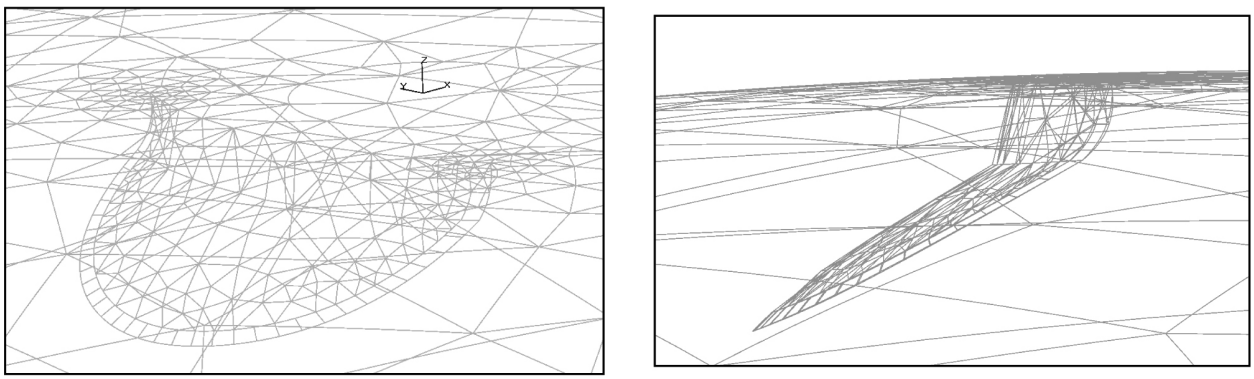

Fig. 4. Model of a ring crack and division into elements after introducing a crack in the ball model (boundary element method)

Rys. 4. Model pęknięcia i podział na elementy po wprowadzeniu pęknięcia do modelu kulki (metoda elementów brzegowych)

The numerical analysis performed with the boundary element method used the following assumptions:

- The material under analysis was assumed to be linear-elastic, which, in the case of silicon nitride, is close to reality.
- The direction of crack propagation was determined by using the strain energy density method (Sih's theory), which means that propagation takes place within the area of relatively minimum amount of strain energy density.
- The value of the critical stress intensity factor for the first loading mode was assumed as KIC = 6 [MPa*m$^{1/2}$] (9).
- Because of a mixed loading mode the effective stress intensity, factor K_{eff} was calculated from Equation (1) (For a thorough analysis of modes used to determine the effective stress intensity factor refer to monograph **[L. 6]**).

$$K_{eff} = \sqrt{K_I{}^2 + K_{II}{}^2 + K_{III}{}^2} \tag{1}$$

- The level of crack increment was determined from Equation (2):

$$\Delta a = \Delta a_{\max}\left(\frac{\Delta K_{\text{eff}}}{\Delta K_{\text{effmax}}}\right)^m \tag{2}$$

where

K_{eff} – effective stress intensity factor [MPa*m$^{1/2}$],
K_I – stress intensity factor for the first loading mode [MPa*m$^{1/2}$],
K_{II} – stress intensity factor for the second loading mode [MPa*m$^{1/2}$],
K_{III} – stress intensity factor for the third loading mode [MPa*m$^{1/2}$],
Δa – crack increment value [mm],
Δa_{max} – maximum crack increment value [mm],
ΔK_{eff} – scope of change in the effective stress intensity factor value [MPa*m$^{1/2}$],
ΔK_{effmax} – maximum value of the effective stress intensity factor change [MPa*m$^{1/2}$],
m – material constant from Paris' law equation (for silicon nitride 18 was assumed according to **[L. 9]**).

- Stress intensity factors were calculated by using J-integral method (the distribution of points along the crack face, where the J-integral contour was led, is shown in **Fig. 5**).

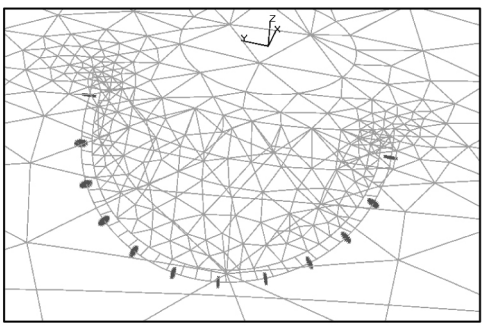

Fig. 5. Location along the point crack face, for which the *J*-integral contour was led

Rys. 5. Położenie wzdłuż czoła pęknięcia punktów, dla których prowadzono kontur całki *J*

The numerical analysis of crack propagation using the boundary element method (BEM) was performed for selected crack locations in relation to the interface of balls. The crack location was defined based on a standardised angle γ/γ_o defined as in **Fig. 6**.

The BEM analysis was performed for specific two crack locations chosen based on the history of changes in stress intensity factor value calculated by using the boundary element method presented in previous publications **[L. 5, 10]**:

- $\gamma/\gamma_o = -1.5$ (**Fig. 7a**, location of the crack with the maximum value of effective stress intensity factor K_I),
- $\gamma/\gamma_o = -0.5$ (**Fig. 7b**, selected location, where $K_I = 0$, while $|K_{II}|>0$ and $|K_{III}|>0$).

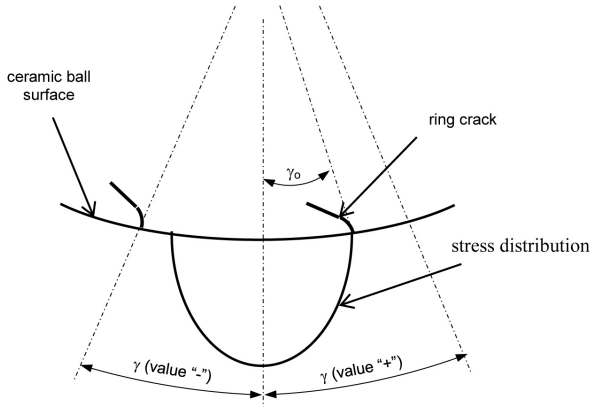

Fig. 6. Method for defining a standardised angle γ/γ_o used to specify the location of a crack

Rys. 6. Sposób definiowania normalizowanego kąta γ/γ_o określającego położenie pęknięcia

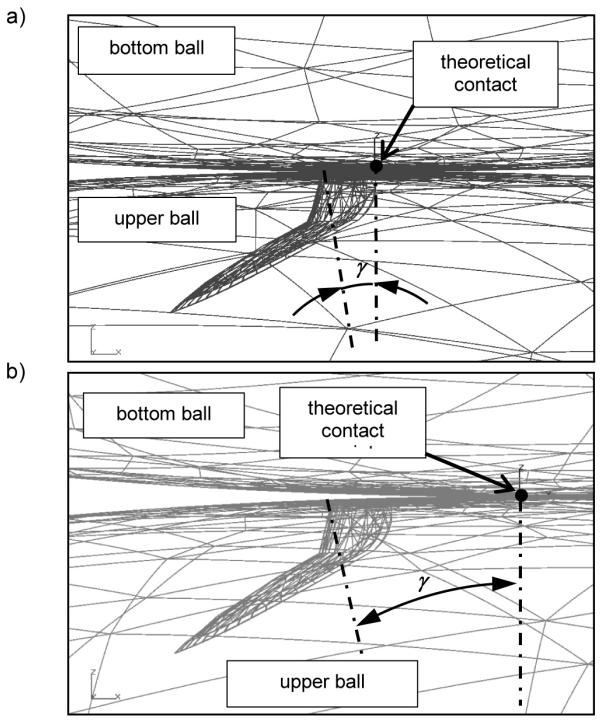

Fig. 7. Crack location in relation to the theoretical ball contact point: a) $\gamma/\gamma_o = -0.5$, b) $\gamma/\gamma_o = -1.5$

Rys. 7. Położenie pęknięcia w stosunku do teoretycznego punktu styku kulek: a) $\gamma/\gamma_o = -0{,}5$, b) $\gamma/\gamma_o = -1{,}5$

IMPACT OF OIL IN THE GAP ON THE CRACK PROPAGATION PROCESS

In the above presented material data, the values and the shape of cracks are consistent enough to allow a comparison with the previously performed experimental studies **[L. 6, 7]**. During the experimental studies, the combined balls were immersed in oil; therefore, the numerical analysis required modelling its impact on the propagation process. This impact depends on many factors, including the shape of the crack, the velocity of liquid inflow into the gap, the size of stress field in relation to the size of crack, the amount of oil trapped in the gap at the moment of gap closure under any external load, etc. The literature describes various models of liquid impact on the crack propagation process in a rolling contact **[L. 11–13]** that allow us to isolate three cases.

Case one is where propagation results from cyclic changes in shear stresses (the second crack mode) contacting the crack surface. The fluid lubricates the crack surface, but it does not exert pressure on the crack surface. Stress intensity factor $K_I = 0$, while the value of friction coefficient between crack surfaces affects the value of stress intensity factor K_{II}.

Case two is where fluid penetrates the gap. It is forced into the gap under load, thus dividing the crack surfaces as a result of fluid action. Fatigue cracks develop as a result of mixed load mode. The maximum values of stress intensity factor K_I and K_{II} occur when the moving interface area overlaps the place where the crack contacts the surface.

Case three is where fluid is trapped in the gap when the crack closes in the place of its contact with the surface or when fluid becomes "sealed" as a result of contact between the crack surface fragments. Fluid trapped in the gap prevents the partial closure of the crack. In this case, the prevailing crack mode is the first K_I mode.

The selection of proper model involves gap closure during stress field displacement. This analysis for a ring crack was performed in paper **[L. 10]**, showing that liquid can impact the crack propagation process through the first two mechanisms.

Case one requires defining a friction coefficient between crack surfaces. The numerical analysis assumed a friction coefficient value of 0.1. Case two requires defining the pressure of liquid acting on the crack surfaces. In the case of flat model, the most frequently assumed value equals the value of contact pressures at the interface between crack and surface **[L. 11]** that is defined by Equation (3).

It is much more difficult to determine the value of pressure acting on crack surfaces by using a 3D model. It is not only due to the impact of stress field at the interface of combined bodies, but also to the opportunity to release fluid from the crack along the crack surface. This numerical analysis assumes that the value of pressure equals the average surface pressure between Points A and B (the points are shown in **Fig. 8**). Because the pressure value in Point B is zero, the pressure value of half of the maximum pressure values in Point A was assumed, i.e. 2.4 GPa.

$$p(x) = p_o\sqrt{1-\left(\frac{x}{a}\right)^2} \tag{3}$$

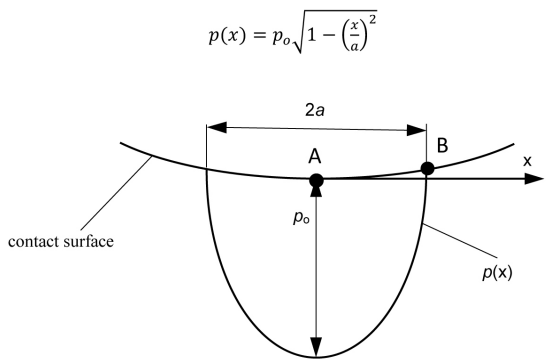

Fig. 8. Symbols as per formula (3)
Rys. 8. Oznaczenia zgodne ze wzorem (3)

NUMERICAL ANALYSIS RESULTS, DISCUSSION

Figure 9 shows the direction of crack propagation for a standardised angle $\gamma/\gamma_o = -1.5$, i.e. for the case when all the three values of stress intensity factors K_I, K_{II}, and K_{III} occur along the crack face. As mentioned above, the direction of propagation was defined in accordance with the direction of minimum strain energy density. **Fig. 9** shows that the direction of gap propagation is not constant and depends on the location along the crack face.

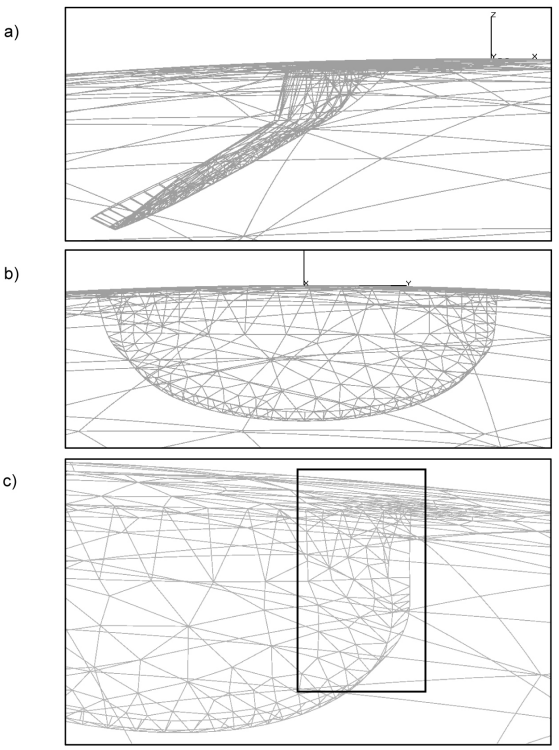

Fig. 9. The propagation direction of a ring crack (Si_3N_4/steel combination, $\gamma/\gamma_o = -1.5$, friction coefficient between gap surfaces of 0.1)
Rys. 9. Kierunek propagacji pęknięcia kolistego (skojarzenie Si_3N_4/stal, $\gamma/\gamma_o = -1{,}5$, współczynnik tarcia pomiędzy powierzchniami szczeliny 0,1)

The direction value for $\gamma/\gamma_o = -1.5$ determined by the propagation angle is presented in **Fig. 10.** The values shown in the horizontal axis of the graph refer to the value of direction in a specific face place as per **Fig. 11.** The graph shows clearly that the propagation direction along the crack face determined by the values ranging from 0.2−0.8 is roughly constant (approximately 60−70 degrees), but it changes considerably when the crack face approaches the surface of ceramic ball (values range 0−0.2 and 0.8−1 along crack face). This area is marked in **Fig. 9c**. It should be noted that propagation in the middle part of the crack face occurs towards the ceramic ball surface.

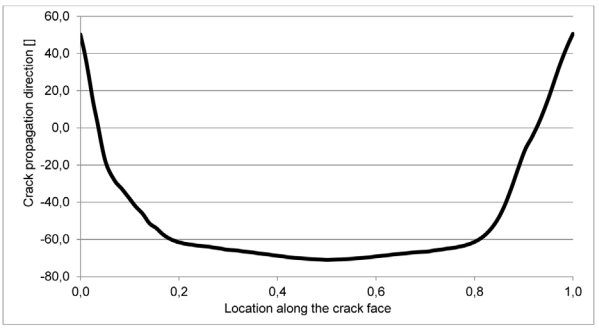

Fig. 10. The propagation direction of a ring crack (Si_3N_4/steel combination, $\gamma/\gamma_o = -1.5$, friction coefficient between gap surfaces of 0.1)
Rys. 10. Kierunek propagacji pęknięcia kolistego (skojarzenie Si_3N_4/stal, $\gamma/\gamma_o = -1{,}5$, współczynnik tarcia pomiędzy powierzchniami szczeliny 0,1)

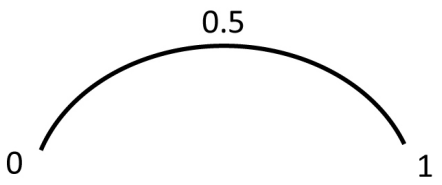

Fig. 11. Ring crack "path" along the crack face with marked locations used in graphs presenting the directions of crack propagation
Rys. 11. „Ścieżka" pęknięcia kolistego wzdłuż czoła pęknięcia z oznaczeniami położenia zastosowanymi na wykresach przedstawiających kierunki propagacji pęknięć

Figures 12 and 13 present the crack propagation direction for standardised angle $\gamma/\gamma_o = -0.5$. Because of the fact that, in Point 0.5 on the crack face, only a factor for the second load mode is available, and the propagation direction nears 90 degrees. Moving away from location 0.5 results in a slight direction change, depending on the presence of K_{III} stress intensity factor. As shown in **Fig. 12**, the propagation direction leads inside the ceramic ball.

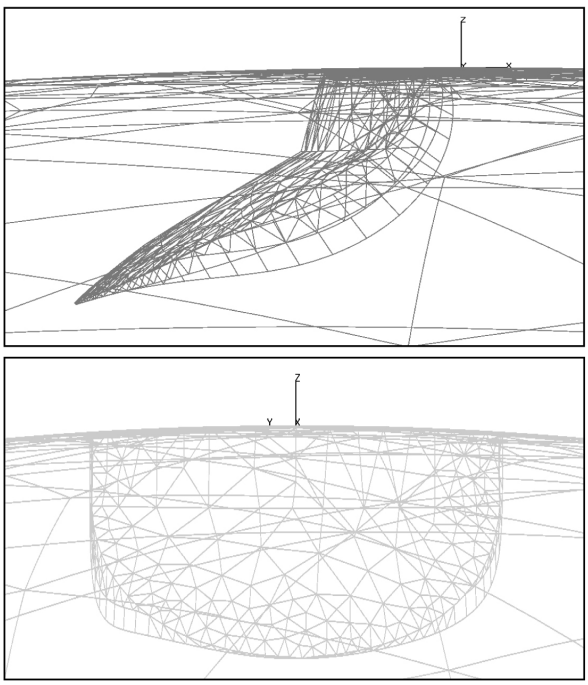

Fig. 12. The propagation direction of a ring crack (Si_3N_4/steel combination, $\gamma/\gamma_o = -0.5$, friction coefficient between gap surfaces of 0.1)

Rys. 12. Kierunek propagacji pęknięcia kolistego (skojarzenie Si_3N_4/stal, $\gamma/\gamma_o = -0,5$, współczynnik tarcia pomiędzy powierzchniami szczeliny 0,1)

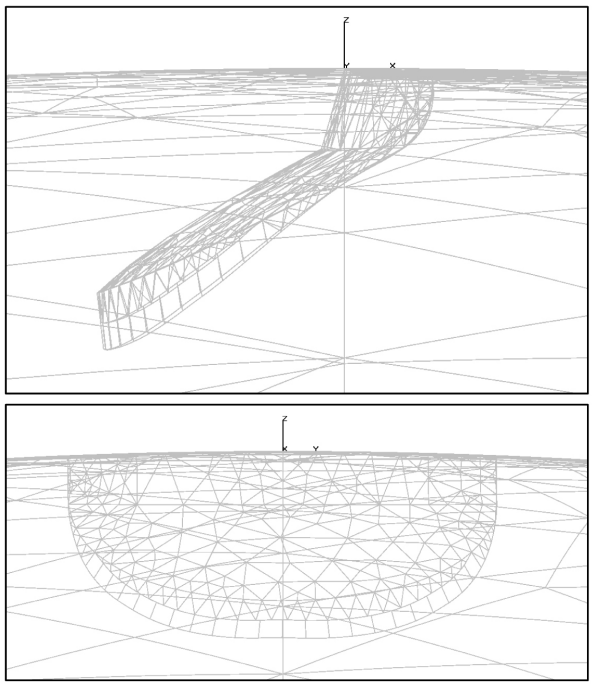

Fig. 14. The propagation direction of a ring crack – increment 1 (Si_3N_4/steel combination, $\gamma/\gamma_o = -0.5$, oil pressure is present between gap surfaces)

Rys. 14. Kierunek propagacji pęknięcia kolistego – przyrost 1 (skojarzenie Si_3N_4/stal, $\gamma/\gamma_o = -0,5$, obecność ciśnienia oleju pomiędzy powierzchniami szczeliny)

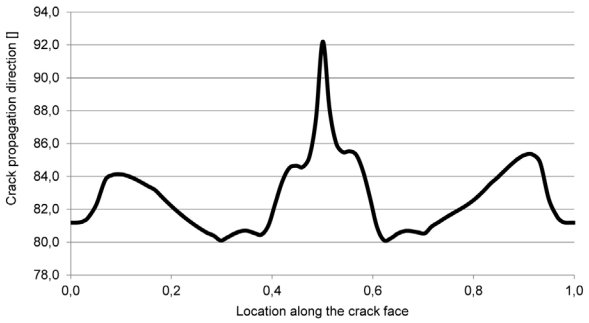

Fig. 13. The propagation direction of a ring crack (Si_3N_4/steel combination, $\gamma/\gamma_o = -0.5$, friction coefficient between gap surfaces of 0.1)

Rys. 13. Kierunek propagacji pęknięcia kolistego (skojarzenie Si_3N_4/stal, $\gamma/\gamma_o = -0,5$, współczynnik tarcia pomiędzy powierzchniami szczeliny 0,1)

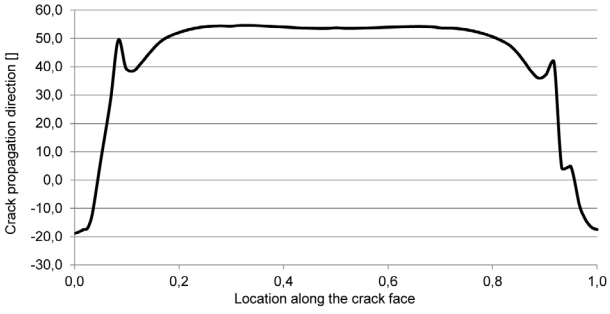

Fig. 15. The propagation direction of a ring crack (Si_3N_4/steel combination, $\gamma/\gamma_o = -0.5$, oil pressure is present between gap surfaces)

Rys. 15. Kierunek propagacji pęknięcia kolistego (skojarzenie Si_3N_4/stal, $\gamma/\gamma_o = -0,5$, obecność ciśnienia oleju pomiędzy powierzchniami szczeliny)

Figures 14 and 15 show the crack propagation direction for standardised angle $\gamma/\gamma_o = -0.5$, this time for the case with oil pressure affecting the crack pressure. The propagation direction along the middle part of crack is constant and equals around 50 degrees, but it changes as the crack face approaches the ceramic ball surface.

COMPARING THE RESULTS OF NUMERICAL ANALYSIS WITH EXPERIMENTAL STUDIES

The experimental studies of ring crack propagation (Hertz type) in silicon nitride balls in rolling contact have been presented in many previous literature items **[L. 6–8, 14]**. Therefore, we are not going to describe them in detail here.

The analysis of crack propagation directions by using the boundary element method is consistent with the experiments performed. The most dangerous propagation direction for the life of combined rolling materials is the one towards the ceramic ball surface. This crack, after reaching the surface, results in considerable cavities ("chipping") in ceramic material between the primary crack and the secondary crack propagating towards the surface of the ceramic ball **[L. 7]**. Examples of photos presenting the surfaces of silicon nitride balls are shown in **Figs. 16 and 17**. The photograph from **Fig. 16** was taken after interrupting an experimental test when the secondary crack reached the ceramic ball surface. The photograph from **Fig. 17** was taken after interrupting an experimental test when "chipping" cavity in ceramic material was detected between the primary and secondary crack. It clearly shows the exposed surface of the primary crack. In practice, such extended cracks result in immediate destruction of the rolling bearing, because of the large amount of hard wear products that appear at the interface between ceramic balls and races.

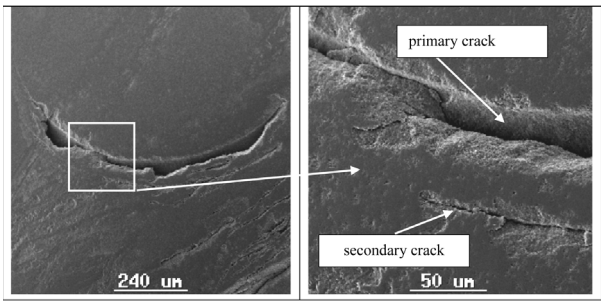

Fig. 16. Photos of a ceramic ball surface showing the propagation of ring cracks on a silicon nitride ball [L. 6]

Rys. 16. Zdjęcia powierzchni kulki ceramicznej obrazujące propagację pęknięć kolistych na kulce z azotku krzemu **[L. 6]**

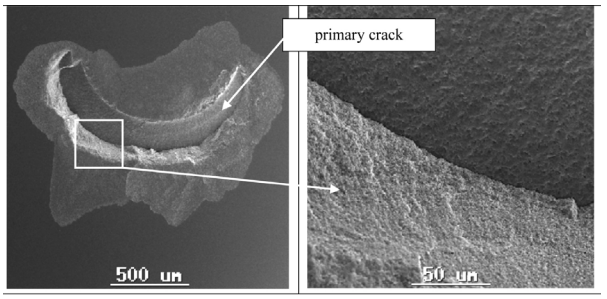

Fig. 17. Photos of a ceramic ball surface showing the propagation of ring cracks on a silicon nitride ball [L. 6]

Rys. 17. Zdjęcia powierzchni kulki ceramicznej obrazujące propagację pęknięć kolistych na kulce z azotku krzemu **[L. 6]**

SUMMARY

The paper presents a numerical analysis using the boundary element method (BEM) of ring cracks (Hertz type) performed on balls made of silicon nitride. Such cracks are commonly found on the surfaces of commercially available ceramic balls and can be caused by shock loads, which sometimes happens during rolling bearing operation.

The numerical analysis shows that the propagation direction for ring cracks depends on the location of gap in relation to the theoretical contact point of combined balls. This direction is not only inconstant in relation to crack location, but it also depends on the place of analysis along the crack face. The crack propagation directions obtained are consistent with data acquired in the previously performed experimental studies. In addition, comparing the numerical analysis with experimental studies can lead us to the conclusion that the most dangerous phenomenon is that of crack propagation towards the ceramic ball surface resulting in large cavities in ceramic material significantly reducing the life of rolling material combinations.

REFERENCES

1. Durazo-Cardenasa I., Starra A., Sousab R., Ferreirab J., Motab A., Kramc M., Hughesd G., Bytnard P., Bele F.: Towards health monitoring of hybrid ceramic bearings in aircraft starter/generators. Procedia Manufacturing, vol. 19, 2018, pp. 50–57.
2. Gabelli A., Morales-Espejel G.E.: A model for hybrid bearing life with surface and subsurface survival. Wear, vol. 422–423, 2019, pp. 223–234.
3. Karaszewski W.: Wytrzymałość zmęczeniowa materiałów ceramicznych – przegląd literatury. (Fatigue strength of ceramic materials – a literature overview.) Tribologia, No. 35(3), 2004, pp. 169–178.
4. Beasy, https://www.beasy.com/crack-growth-simulation.html, software developer website [access as of 2 June 2019].
5. Portela A., Aliabadi M., Rooke D.: Dual boundary element analysis of crack propoagation. Computers & Structures, vol. 2, no 46, 1993, pp. 237–247.

6. Karaszewski W.: Badanie wpływu wybranych czynników na trwałość ceramicznych elementów łożysk tocznych (Assessing the impact of selected factors on the life of ceramic rolling bearing elements.), Wydawnictwo Politechniki Gdańskiej (Publishing Unit of the Gdańsk University of Technology), Gdańsk, 2013.
7. Karaszewski W.: The influence of oil additives on spread cracks in silicon nitride, Tribology International, vol. 41, issue 9–10, 2008, pp. 889–895.
8. Karaszewski W.: Analysis of Ceramic Elements with Ring-Crack Defects in Lubricated Rolling Contact, Solid State Phenomena, vol. 250, 2016, pp. 43–49.
9. Bar-On I., Beals J., Kitagawa H., Tanaka T.: Faitgue 90: Proceedings of 4th International Conference on Fatigue and Fatigue Thresholds. Honolulu, Hawai: Materials and Component Engineering Publications, Limited, vol. 2, 1990, pp. 793–798.
10. Karaszewski W.: Hertzian Crack Propagation in Ceramic Rolling Elements, Key Engineering Materials, vol. 598, 2014, pp. 92–98.
11. Bogdański S., Lewicki P., Szymaniak M.: Experimental and theoretical investigation of the phenomenon of filling the RCF crack with liquid. Wear, vol. 258, 2005, pp. 1280–1287.
12. Glodez S., Potocnik R., Flasker J., Zafosnik B.: Numerical modeling of crack path in the lubricated rolling-sliding contact problems. Engineering Fracture Mechanics, vol. 75, 2008, pp. 880–891.
13. Lewicki P., Bogdański S.: 3D model of liquid entrapment mechanism for rolling contact fatigue cracks in rails. Wear, vol. 265, 2008, pp. 1356–1362.
14. Wang Y., Hadfield M.: Failure modes of ceramic rolling elements with surface crack defects, Wear 256, 2004, pp. 208–219.